GEOLOGY | THE GEOLOGICAL SOCIETY OF AMERICA®

https://doi.org/10.1130/G52435.1

Manuscript received 12 December 2023
Manuscript accepted 18 June 2024

Published online 30 July 2024

Volcanic and orbitally forced carbon release during the Middle Eocene Climatic Optimum

Yiquan Ma[1,2,*], Majie Fan[3], Chen Zhang[1,2,*], Stephen E. Grasby[4], Runsheng Yin[5], Yangbo Lu[6], Bolin Zhang[1,2], Xin Jin[1,2], Chao Ma[1,2], Yongchao Lu[6], and Appy Sluijs[7]

[1]State Key Laboratory of Oil and Gas Reservoir Geology and Exploitation & Institute of Sedimentary Geology, Chengdu University of Technology, Chengdu 610059, China
[2]Key Laboratory of Deep-time Geography and Environment Reconstruction and Applications of Ministry of Natural Resources, Chengdu University of Technology, Chengdu 610059, China
[3]Department of Earth and Environmental Sciences, The University of Texas at Arlington, Arlington, Texas 76019, USA
[4]Department of Earth, Energy, and Environment, University of Calgary, Calgary, Alberta T2N 1N4, Canada
[5]State Key Laboratory of Ore Deposit Geochemistry, Institute of Geochemistry, Chinese Academy of Sciences, Guiyang 550081, China
[6]College of Earth Resources, China University of Geosciences, Wuhan 430074, China
[7]Department of Earth Sciences, Faculty of Geoscience, Utrecht University, 3584 CB Utrecht, Netherlands

ABSTRACT

The drivers of the Middle Eocene Climatic Optimum (MECO) remain enigmatic. Here we report a high-resolution terrestrial MECO record from the Bohai Bay Basin, eastern China. The record shows episodic Hg enrichments and a volcanogenic Δ^{199}Hg signature during the MECO, and an abrupt chemical weathering enhancement and negative $\delta^{13}C_{org}$ excursion (CIE) during the MECO peak warmth. A high-resolution age model constrains the MECO to ca. 40.59–40.18 Ma with the onset in the first ~320 k.y. Peak warmth and the CIE initiated at 40.27 Ma, corresponding to 405 k.y. and 100 k.y. eccentricity maxima, and lasted for ~90 k.y., reminiscent of the early Eocene hyperthermals. Our findings suggest that episodic volcanism contributed to gradual atmospheric pCO_2 rise, leading to the long duration of the MECO onset. Orbital forcing at 40.27 Ma, on top of CO_2 forcing, caused the peak warmth and a positive carbon cycle feedback. The regional increase in weathering is inconsistent with evidence for weakened global continental weathering, suggesting strong spatial heterogeneity in the weathering response to MECO warming.

INTRODUCTION

The Middle Eocene Climatic Optimum (MECO) was a global warming event at ca. 40 Ma that briefly interrupted a long-term cooling of the climate (Fig. 1A). It was identified in marine carbonate records as an initial $\delta^{18}O$ drop (i.e., MECO onset) around the middle of Chron C18r, followed by a negative $\delta^{18}O$ excursion peak that lasted for nearly 100 k.y. (i.e., the peak MECO) at the base of Chron C18n.2n, and a rapid return to pre-event value within the next ~50 k.y. (e.g., Bohaty et al., 2009). Marine records show clear environmental perturbations during the MECO, including a rise in atmospheric pCO_2, warming in surface and intermediate deep-water, changes in biodiversity, and shallowing of the calcite compensation depth (e.g., Bohaty et al., 2009; Bijl et al., 2010; Henehan et al., 2020). On MECO time scales, these observations are inconsistent with the predictions of conventional carbon cycle theory (Sluijs et al., 2013) and geochemical evidence of a globally weak continental silicate weathering feedback (van der Ploeg et al., 2018; Krause et al., 2023).

Limited terrestrial MECO studies suggest strong spatial heterogeneity in temperature and hydrological response to the MECO (e.g., Bosboom et al., 2014; Methner et al., 2016), and this is at least partly attributable to uncertainties in age assessment and even the lack of positive identification of the MECO. Very promising from this perspective is a lacustrine sequence (ca. 41.11–39.69 Ma) in the Bohai Bay Basin, eastern China, that encompasses the MECO based on a robust magneto-cyclostratigraphy age model that integrated biostratigraphy and radiometric ages of volcanic layers (Fig. 1B; Ma et al., 2023). This detailed chronology provides a unique opportunity to further our documentation of climate and carbon cycle dynamics across the MECO. Here we conduct a high-resolution geochemical study on these rocks to locate the MECO and understand the continental environmental change and driving mechanism of the MECO warming.

METHODS AND RESULTS

We conducted high-resolution sampling from the third member (Es3) of the Shahejie Formation of the FY1 core in the Bohai Bay Basin (37°15′11.29″N, 118°02′13.27″E; Fig. 1C), of which the lower unit of Es3 encompasses the MECO (Fig. 2). These samples were analyzed for mercury (Hg), total organic carbon (TOC) and total sulfur (TS) concentrations, chemical index of alteration (CIA), $\ln(Al_2O_3/Na_2O)$, Hg and organic carbon ($\delta^{13}C_{org}$) isotopic compositions, and maceral compositions. Detailed descriptions of the geological setting and sample analysis are in the Supplemental Material[1].

Yiquan Ma https://orcid.org/0000-0002-0937-9366
*mayiquan@cdut.edu.cn; zhangchen2022@cdut.edu.cn

[1]Supplemental Material. Detailed geological setting, methods and results, host phases of mercury, error propagations for derivative proxies, evaluation of the negative carbon isotope excursion, and supplemental figures. Please visit https://doi.org/10.1130/GEOL.S.26072710 to access the supplemental material; contact editing@geosociety.org with any questions.

CITATION: Ma, Y., et al., 2024, Volcanic and orbitally forced carbon release during the Middle Eocene Climatic Optimum: Geology, v. 52, p. 813–818, https://doi.org/10.1130/G52435.1

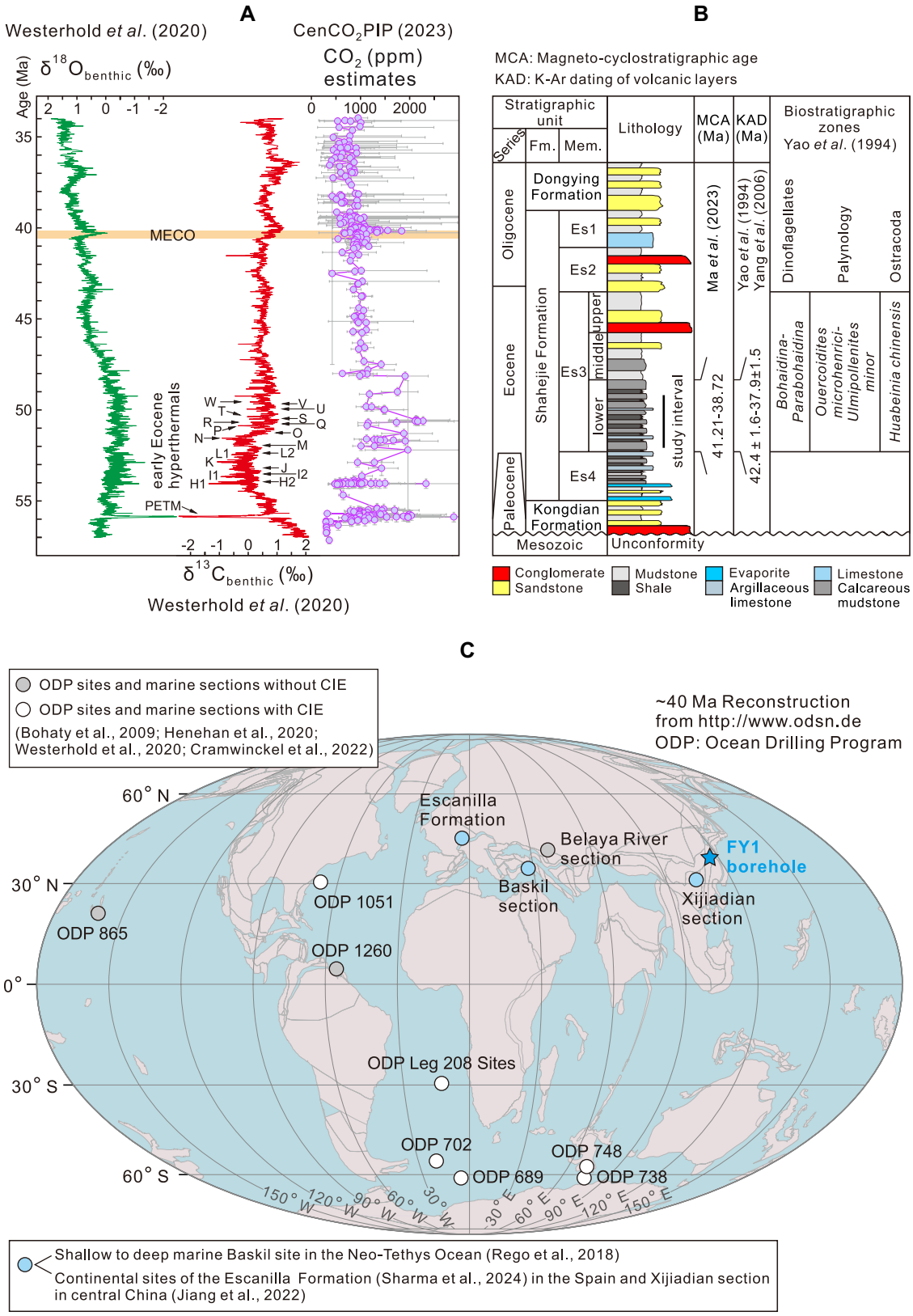

Figure 1. (A) Eocene paleoclimate records of benthic foraminifer $\delta^{13}C$ and $\delta^{18}O$ and atmospheric pCO_2. CenCO$_2$PIP (2023)—Cenozoic CO_2 Proxy Integration Project Consortium (2023); PETM—Paleocene–Eocene Thermal Maximum. (B) Generalized stratigraphic column and age constraints of the middle Eocene rocks in the Bohai Bay Basin, modified from Ma et al. (2023). (C) Paleogeographic map (ca. 40 Ma) showing the locations of the FY1 borehole and other Middle Eocene Climatic Optimum (MECO) sites mentioned in the study. CIE—carbon isotope excursion.

A total of 352 Hg anomaly values (Hg_{EF}), calculated as Hg/TOC, Hg/TS, and Hg/Al ratios, were superimposed to interpret the Hg signal (see Supplemental Material for details). The Hg_{EF} shows several spikes with negligible data uncertainties. The majority of the Hg_{EF} spikes, after error propagation, are >2, showing significant Hg enrichment over the background level (cf. Shen et al., 2019). The $\ln(Al_2O_3/Na_2O)$ and CIA data and their comparison with marine carbonate stable isotope data were used to divide the studied interval into three segments (Figs. 2 and 3). The interval below 3202 m (before ca. 40.59 Ma) is marked by low and relatively stable $\ln(Al_2O_3/Na_2O)$ and CIA values, slight increase of $\delta^{13}C_{org}$, and low Hg_{EF} (<2) with a few spikes up to 4.1 near the top. The $\Delta^{199}Hg$, induced by mass-independent fractionation of Hg isotopes (MIF), is

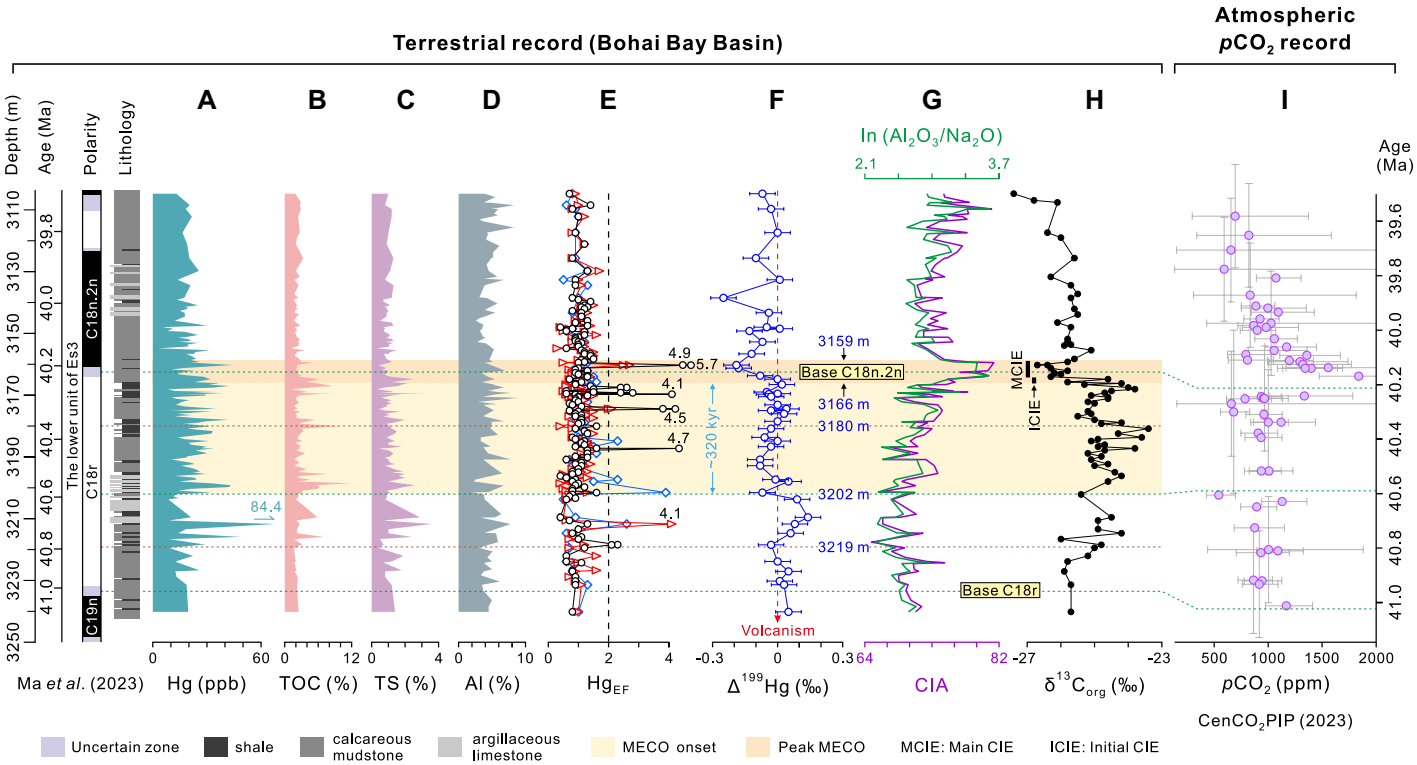

Figure 2. Comparison of proxy data in the FY1 borehole and pCO_2 records across the Middle Eocene Climatic Optimum (MECO). (A) Hg concentrations; (B) total organic carbon (TOC) contents; (C) total sulfur (TS) contents; (D) Al contents; (E) Hg_{EF} calculated with Hg/TOC (triangle), Hg/TS (circle), and Hg/Al (rhombus), respectively; (F) $\Delta^{199}Hg$ values; (G) chemical index of alteration (CIA) and $ln(Al_2O_3/Na_2O)$ values; (H) $\delta^{13}C_{org}$ values; (I) estimated pCO_2. CIE—carbon isotope excursion.

slightly positive (0‰ to +0.05‰) below 3219 m and increases slightly (up to +0.14‰) toward the top of the segment. Between 3202 and 3159 m (ca. 40.59–40.18 Ma) is characterized by a gradual increase of $ln(Al_2O_3/Na_2O)$ and CIA, reaching peaks right above 3166 m (ca. 40.27 Ma), near the base of Chron C18n.2n, and variable Hg concentrations with Hg_{EF} spikes up to 5.7. The $\Delta^{199}Hg$ values are slightly negative at the base, close to zero (mainly −0.04‰ to +0.04‰) between 3180 and 3166 m (ca. 40.36–40.27 Ma), and shift to negative values (to −0.19‰) at the top. A negative carbon isotope excursion (CIE) of ~1.7‰ also occurs at 3166 m. Above 3159 m (after ca. 40.18 Ma) shows low and stable $ln(Al_2O_3/Na_2O)$, CIA, Hg concentrations, and Hg_{EF} values, gradual decrease of $\delta^{13}C_{org}$, and $\Delta^{199}Hg$ values mostly below 0‰. The macerals contain predominantly autochthonous materials of algal origin (e.g., lamalginite) (80.7%–98.7%) with minor vitrinite (1.3%–12.8%) and exinite (≤6.4%).

DISCUSSION

MECO Stratigraphy and Weathering in the Bohai Bay Basin

The base of Chron C18n.2n is the initiation of MECO peak warmth in the marine realm (Bohaty et al., 2009), and the tie point for marine-terrestrial comparison. The trends of our weathering indices and $\delta^{13}C_{org}$ are consistent with marine carbonate $\delta^{18}O$ and $\delta^{13}C$ values (Bohaty et al., 2009; Westerhold et al., 2020) (Fig. 3). At 3202 m (ca. 40.59 Ma), the weathering indices terminate their low and relatively stable trend and begin to gradually increase upward at the onset of a gradual drop of marine $\delta^{18}O$. Between 3202 and 3166 m (ca. 40.59–40.27 Ma), the weathering indices increase gradually during the gradual drop of marine $\delta^{18}O$, which we interpret to reflect the MECO onset. The weathering indices then increase toward the peaks at the base of Chron C18n.2n and return to lows at 3159 m (40.18 Ma), reflecting the peak MECO toward its termination (Fig. 3). Student's t-test applied to the weathering indices for the lower and middle segments yields $p < 0.05$, suggesting a statistically significant difference. These data suggest intensified regional continental silicate weathering in a warm climate, consistent with other terrestrial and marine records in mid-latitude Northern Hemisphere settings (Rego et al., 2018; Jiang et al., 2022). Given evidence for globally stable or decreased continental weathering intensity during the MECO from whole-ocean lithium and osmium isotope ratios (van der Ploeg et al., 2018; Krause et al., 2023) and a sedimentary succession in Spain (Sharma et al., 2024), our data suggest a spatially heterogenous hydrological response to MECO warming.

Orbital Forcing of the Peak MECO

Our study shows a negative CIE during the peak MECO in the terrestrial realm (Fig. 3). Evaluation of this CIE rules out degradation or changes in organic matter type as the cause (see Supplemental Material). A similar peak MECO CIE has been documented in many, but not all, marine records (Figs. 1C and 3). The discovery of this CIE in the terrestrial realm in this study and Europe (Sharma et al., 2024) confirms a global carbon cycle disturbance during the peak MECO associated with massive ^{13}C-depleted carbon input into the ocean-atmosphere system (Bohaty et al., 2009). The robust astrochronology of the studied core (Ma et al., 2023) indicates that the MECO CIE occurred at the orbital conjunction of 405 k.y. long-eccentricity and 100 k.y. short-eccentricity maxima (Fig. 3), suggesting astronomical triggering of the peak MECO warmth.

Hg Evidence for Volcanism before and during the MECO

Mercury (Hg) concentrations and isotopes are useful proxies of volcanism because volcanic degassing is the ultimate natural emission source of Hg to the atmosphere, and Hg is then subsequently deposited on land and oceans, leading to high Hg anomalies in global sediments (Grasby et al., 2019). Mercury isotopes, especially MIF signals ($\Delta^{199}Hg$), have functioned as a tracer of mercury sources in ancient sedimentary systems (Thibodeau et al., 2016; Grasby et al., 2019). MIF occurs mainly via photochemical processes with little interference from other processes and

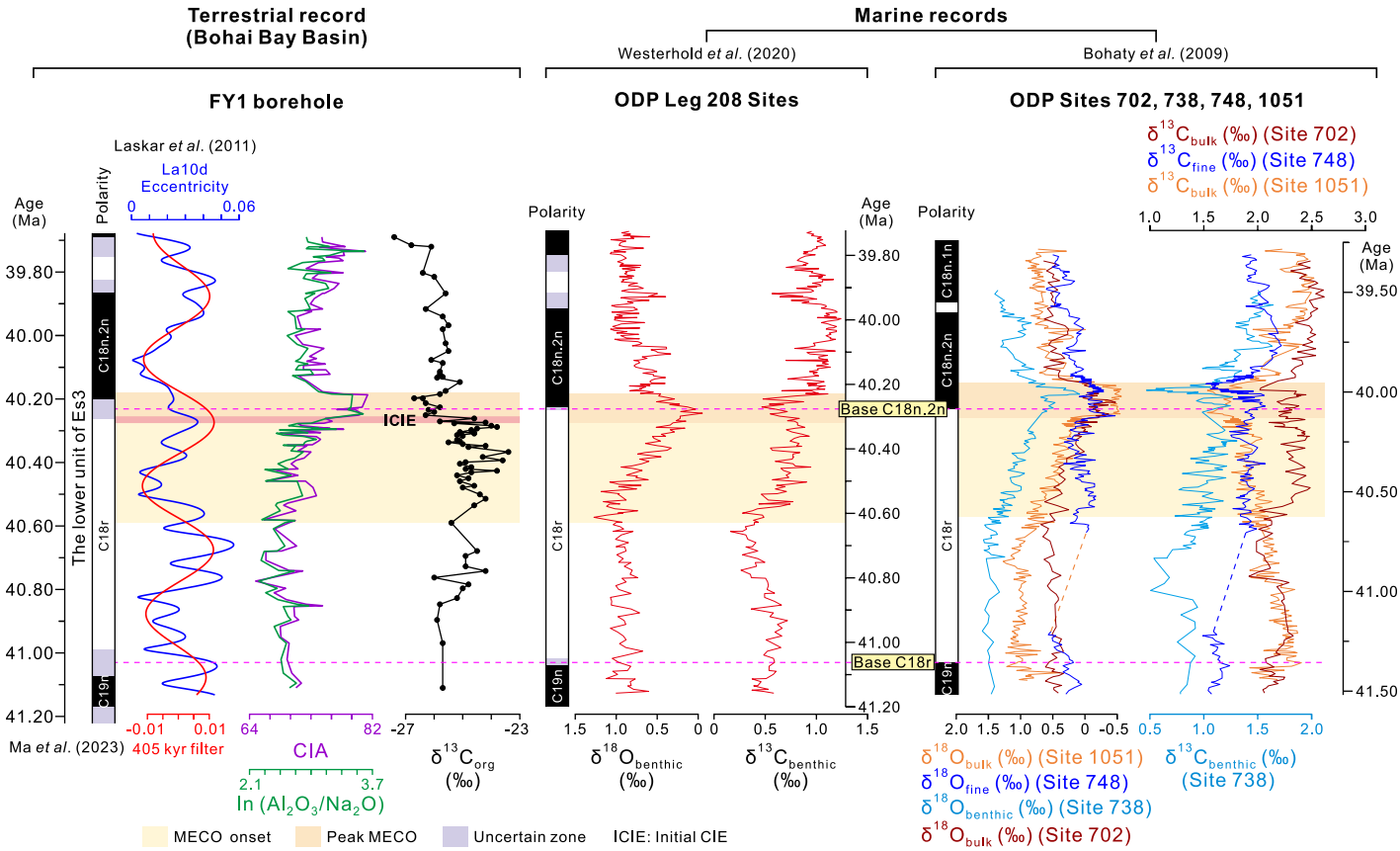

Figure 3. Comparison of the chemical index of alteration (CIA) and $\ln(Al_2O_3/Na_2O)$ and $\delta^{13}C_{org}$ records in this study and eccentricity cycles of the La2010d solution between 41.13 and 39.68 Ma (blue) and its filtered 405 k.y. cycles (red), benthic foraminifer $\delta^{18}O$ and $\delta^{13}C$ data from Ocean Drilling Program (ODP) Leg 208 Sites, and bulk carbonate $\delta^{18}O$ and $\delta^{13}C$ data, benthic foraminifer $\delta^{18}O$ and $\delta^{13}C$ data, and fine-fraction carbonate $\delta^{18}O$ and $\delta^{13}C$ data from ODP Sites 1051, 702, 738, and 748, respectively. CIE—carbon isotope excursion; MECO—Middle Eocene Climatic Optimum.

can provide unambiguous source constraints (Blum et al., 2014). Volcanic Hg usually has near-zero MIF signals ($\Delta^{199}Hg \approx 0‰$), but can be modified by Hg(II) photo-reduction process on Earth's surface, resulting in negative $\Delta^{199}Hg$ values in terrestrial fluxes and positive $\Delta^{199}Hg$ values in atmospheric fluxes (Blum et al., 2014). MIF has been used to examine volcanic Hg inputs from large igneous provinces (LIPs) and regional volcanism, and near-zero MIF values have been interpreted as evidence of volcanic Hg inputs that did not undergo photo-reduction during transport (e.g., Thibodeau et al., 2016; Shen et al., 2019; Zhao et al., 2022).

The host phases of Hg in the Bohai Bay Basin include organic matter, sulfides, and clay minerals (see Supplemental Material). The variation of Hg is not related to lithology, and the high Hg concentration is not the result of high TOC during the MECO. Therefore, the Hg peaks provide evidence for some form of mercury influx before and during the MECO warming. Below the MECO onset, the increase of $\Delta^{199}Hg$ relative to the background flux and high Hg peaks imply episodic inputs of volcanically sourced Hg that was chemically photoreduced during the atmospheric pathways (Figs. 2E and 2F). Accumulation of volcanic CO_2 may have eventually pushed atmospheric pCO_2 up, leading to the MECO onset. Our Hg record doesn't extend very far back in time; thus, we acknowledge that longer Hg data sets are required to confirm whether the C18r is particularly anomalous.

During the MECO onset, the slightly negative $\Delta^{199}Hg$ values are coincident with the high Hg_{EF} spikes before ca. 40.36 Ma, suggesting Hg flux dominated by terrestrial erosion and/or volcanically derived Hg came via terrestrial runoff (Figs. 2E and 2F). After ca. 40.36 Ma, the temporally uniform near-zero $\Delta^{199}Hg$ values with multiple high Hg_{EF} spikes (to 4.5) suggest dominant inputs of volcanic Hg that lacks MIF (Figs. 2E and 2F). Although near-zero $\Delta^{199}Hg$ might also have been produced through mixing of atmospheric-sourced and terrestrial-sourced Hg, such a mixing process is unlikely to have produced high Hg_{EF} spikes with temporally uniform near-zero $\Delta^{199}Hg$ values (Thibodeau et al., 2016; Zhao et al. 2022). During the peak MECO, the high Hg spikes with Hg_{EF} values up to 5.7 and negative $\Delta^{199}Hg$ values suggest that enhanced Hg inputs are derived from increased terrestrial runoff unrelated to volcanism, or represent increased volcanic output brought in via enhanced terrestrial input (Figs. 2E and 2F; Shen et al., 2019; Them et al., 2019). This elevated terrestrial signal was most likely caused by intensifying regional hydrological cycle during the peak warmth, which enhanced silicate weathering and runoff and washed more terrestrial Hg into the Bohai Bay Basin (Figs. 2F and 2G). Our high Hg spikes are well below those observed for several major mass extinction events that were thought to be triggered by LIP eruptions (Grasby et al., 2019; Racki, 2020), suggesting that volcanism during the MECO was not as intense as those driving mass extinctions. The addition of atmospheric CO_2 from episodic volcanism before and during the MECO did not increase pCO_2 drastically, only rising by 0.55–0.75 doublings at the MECO, suggesting high Eocene climate sensitivity (Henehan et al., 2020).

Four areas of late middle Eocene volcanism may have contributed to the Hg signals observed, including the Azerbaijan-Bazman Arc (van der Boon et al., 2021), Pacific rim, East Africa Rift zone, and North Atlantic mid-ocean ridge (van der Ploeg et al., 2018, and references therein). Timing and magnitude of these eruptions are not well constrained, making it impossible to assess which volcanic center(s) caused the Hg signal in the Bohai Bay Basin. Volcanism in Africa and the Atlantic are very far from eastern China,

and volcanism in a submarine spreading ridge is less likely to contribute large amounts of Hg to the atmosphere. Cenozoic volcanism in eastern China was predominantly driven by the subduction of the Pacific Plate and is part of the Pacific Rim subduction zone volcanism (e.g., Zhang et al., 2023). Therefore, the eruptions of the Azerbaijan-Bazman Arc and Pacific rim are the most likely Hg sources. However, a Hg anomaly was not observed in the organic-rich sediments in the northern Peri-Tethys during the MECO when the basin experienced local restriction and euxinia (Cramwinckel et al., 2022), which may be related to the effectiveness of different depositional environments and/or sediment types in recording Hg anomalies, and anoxic conditions (e.g., Frieling et al., 2023). Additional Hg records and knowledge of the timing and Hg dispersal efficiency of related volcanoes and their perturbance to global Hg cycle are needed to further test this hypothesis of a volcanic driver of MECO.

Comparison with Early Eocene Hyperthermals

The MECO peak warmth has a short duration (~90 k.y. as shown in this study), like the Paleocene–Eocene Thermal Maximum (PETM) and at least 20 suspected and documented early Eocene transient global warming events, termed hyperthermals (Fig. 1A; e.g., Westerhold et al., 2018, 2020). All the hyperthermals, perhaps except for the PETM, were driven by orbital forcing, as they correspond to eccentricity maxima (e.g., Lourens et al., 2005; Westerhold et al., 2018), and exhibit mathematical characteristics of Earth system tipping points (Setty et al., 2023). The North Atlantic Igneous Province may have comprised an important carbon source for long-term late Paleocene–early Eocene warming (Eldholm and Thomas, 1993) and perhaps even for the PETM (e.g., Frieling et al., 2016). From this perspective, there may be an analogy between long-term late Paleocene–early Eocene warming and MECO warming, both triggering a strong nonlinear carbon cycle response during eccentricity maxima, causing "hyperthermals" for the early Eocene and "peak warmth" for the MECO. However, the longer MECO onset than the early Eocene hyperthermals, based on this study, may be a result of slow and episodic volcanic CO_2 release prior to the peak warmth. The lower Hg_{EF} magnitude during the MECO compared to the PETM (Jin et al., 2024) suggests that the intensity of volcanism during the MECO was lower than PETM. Collectively, we suggest that the long-term MECO warming driven by CO_2 forcing and orbital conjunction at 40.27 Ma pushed the climate system toward a tipping point that eventually triggered massive carbon release from permafrost and/or methane hydrates, as proposed previously for the early Eocene hyperthermal events (e.g., DeConto et al., 2012; Lourens et al., 2005).

CONCLUSIONS

We identified the MECO onset and peak warmth in an orbitally tuned lacustrine section in the Bohai Bay Basin, eastern China. Our Hg data show evidence of episodic volcanism right before and during the MECO, suggesting that the slow and gradual addition of volcanic CO_2 increased atmospheric pCO_2 and triggered the long duration of the MECO onset. The MECO peak warmth started at a 405 k.y. and 100 k.y. eccentricity maxima, in association with a CIE and enhanced weathering, suggesting that peak warmth was triggered by orbital forcing on top of long-term CO_2 forcing, similar to the early Eocene hyperthermals. We also documented a regional increase of continental weathering in response to MECO warming, inconsistent with the global trends, suggesting strong spatial heterogeneity.

ACKNOWLEDGMENTS

We thank the Shengli Oilfield Company (SINOPEC) for providing samples. This work was supported by the National Natural Science Foundation of China (grants 42172181, 41802175) and the Natural Science Foundation of Sichuan Province (grant 2022NSFSC1075) We thank editor Urs Schaltegger and five anonymous reviewers for valuable and constructive comments.

REFERENCES CITED

Bijl, P.K., Houben, A.J.P., Schouten, S., Bohaty, S.M., Sluijs, A., Reichart, G.-J., Sinninghe Damste, J.S., and Brinkhuis, H., 2010, Transient middle Eocene atmospheric CO_2 and temperature variations: Science, v. 330, p. 819–821, https://doi.org/10.1126/science.1193654.

Blum, J.D., Sherman, L.S., and Johnson, M.W., 2014, Mercury isotopes in Earth and environmental sciences: Annual Review of Earth and Planetary Sciences, v. 42, p. 249–269, https://doi.org/10.1146/annurev-earth-050212-124107.

Bohaty, S.M., Zachos, J.C., Florindo, F., and Delaney, M.L., 2009, Coupled greenhouse warming and deep-sea acidification in the middle Eocene: Paleoceanography, v. 24, https://doi.org/10.1029/2008PA001676.

Bosboom, R.E., Abels, H.A., Hoorn, C., van den Berg, B.C.J., Guo, Z., and Dupont-Nivet, G., 2014, Aridification in continental Asia after the Middle Eocene Climatic Optimum (MECO): Earth and Planetary Science Letters, v. 389, p. 34–42, https://doi.org/10.1016/j.epsl.2013.12.014.

Cenozoic CO_2 Proxy Integration Project ($CenCO_2PIP$) Consortium, 2023, Toward a Cenozoic history of atmospheric CO_2: Science, v. 382, https://doi.org/10.1126/science.adi5177.

Cramwinckel, M.J., van der Ploeg, R., van Helmond, N.A.G.M., Waarlo, N., Agnini, C., Bijl, P.K., van der Boon, A., Brinkhuis, H., Frieling, J., Krijgsman, W., Mather, T.A., Middelburg, J.J., Peterse, F., Slomp, C.P., and Sluijs, A., 2022, Deoxygenation and organic carbon sequestration in the Tethyan realm associated with the middle Eocene climatic optimum: Geological Society of America Bulletin, v. 135, p. 1280–1296, https://doi.org/10.1130/B36280.1.

DeConto, R.M., Galeotti, S., Pagani, M., Tracy, D., Schaefer, K., Zhang, T., Pollard, D., and Beerling, D.J., 2012, Past extreme warming events linked to massive carbon release from thawing permafrost: Nature, v. 484, p. 87–91, https://doi.org/10.1038/nature10929; erratum available at https://doi.org/10.1038/nature11424.

Eldholm, O., and Thomas, E., 1993, Environmental impact of volcanic margin formation: Earth and Planetary Science Letters, v. 117, p. 319–329, https://doi.org/10.1016/0012-821X(93)90087-P.

Frieling, J., Svensen, H.H., Planke, S., Cramwinckel, M.J., Selnes, H., and Sluijs, A., 2016, Thermogenic methane release as a cause for the long duration of the PETM: Proceedings of the National Academy of Sciences of the United States of America, v. 113, p. 12,059–12,064, https://doi.org/10.1073/pnas.1603348113.

Frieling, J., Mather, T.A., März, C., Jenkyns, H.C., Hennekam, R., Reichart, G.-J., Slomp, C.P., and van Helmond, N.A.G.M., 2023, Effects of redox variability and early diagenesis on marine sedimentary Hg records: Geochimica et Cosmochimica Acta, v. 351, p. 78–95, https://doi.org/10.1016/j.gca.2023.04.015.

Grasby, S.E., Them, T.R., Chen, Z., Yin, R., and Ardakani, O.H., 2019, Mercury as a proxy for volcanic emissions in the geologic record: Earth-Science Reviews, v. 196, https://doi.org/10.1016/j.earscirev.2019.102880.

Henehan, M.J., Edgar, K.M., Foster, G.L., Penman, D.E., Hull, P.M., Greenop, R., Anagnostou, E., and Pearson, P.N., 2020, Revisiting the Middle Eocene Climatic Optimum "Carbon Cycle Conundrum" with new estimates of atmospheric pCO_2 from boron isotopes: Paleoceanography and Paleoclimatology, v. 35, https://doi.org/10.1029/2019PA003713.

Jiang, H., Zhang, J., Zhang, S., Zhong, N., Wan, S., Alsop, G.I., Xu, H., Guo, Q., and Yan, Z., 2022, Tectonic and climatic impacts on environmental evolution in East Asia during the Palaeogene: Geophysical Research Letters, v. 49, https://doi.org/10.1029/2021GL096832.

Jin, S., Kemp, D.B., Shen, J., Yin, R., Jolley, D.W., Vieira, M., and Huang, C., 2024, Spatiotemporal distribution of global mercury enrichments through the Paleocene-Eocene Thermal Maximum and links to volcanism: Earth-Science Reviews, v. 248, https://doi.org/10.1016/j.earscirev.2023.104647.

Krause, A.J., Sluijs, A., van der Ploeg, R., Lenton, T.M., and Pogge von Strandmann, P.A.E., 2023, Enhanced clay formation key in sustaining the Middle Eocene Climatic Optimum: Nature Geoscience, v. 16, p. 730–738, https://doi.org/10.1038/s41561-023-01234-y; erratum available at https://doi.org/10.1038/s41561-023-01280-6.

Laskar, J., Fienga, A., Gastineau, M., and Manche, H., 2011, La2010: A new orbital solution for the long-term motion of the Earth: Astronomy & Astrophysics, v. 532, A89, https://doi.org/10.1051/0004-6361/201116836.

Lourens, L., Sluijs, A., Kroon, D., Zachos, J.C., Thomas, E., Röhl, U., Bowles, J., and Raffi, I., 2005, Astronomical pacing of late Palaeocene to early Eocene global warming events: Nature, v. 435, p. 1083–1087, https://doi.org/10.1038/nature03814.

Ma, Y., Fan, M., Li, M., Ogg, J.G., Zhang, C., Feng, J., Zhou, C., Liu, X., Lu, Y., Liu, H., Eldrett, J.S., and Ma, C., 2023, East Asian lake hydrology modulated by global sea-level variations in the Eocene warmhouse: Earth and Planetary Science Letters, v. 602, https://doi.org/10.1016/j.epsl.2022.117925.

Methner, K., Mulch, A., Fiebig, J., Wacker, U., Gerdes, A., Graham, S.A., and Chamberlain, C.P., 2016, Rapid Middle Eocene temperature change in western North America: Earth and Planetary Science Letters, v. 450, p. 132–139, https://doi.org/10.1016/j.epsl.2016.05.053.

Racki, G., 2020, A volcanic scenario for the Frasnian-Famennian major biotic crisis and other Late De-

vonian global changes: More answers than questions?: Global and Planetary Change, v. 189, https://doi.org/10.1016/j.gloplacha.2020.103174.

Rego, E.S., Jovane, L., Hein, J.R., Sant'Anna, L.G., Giorgioni, M., Rodelli, D., and Özcan, E., 2018, Mineralogical evidence for warm and dry climatic conditions in the Neo-Tethys (eastern Turkey) during the middle Eocene: Palaeogeography, Palaeoclimatology, Palaeoecology, v. 501, p. 45–57, https://doi.org/10.1016/j.palaeo.2018.04.007.

Setty, S., Cramwinckel, M.J., van Nes, E.H., van de Leemput, I.A., Dijkstra, H.A., Lourens, L.J., Scheffer, M., and Sluijs, A., 2023, Loss of Earth system resilience during early Eocene transient global warming events: Science Advances, v. 9, https://doi.org/10.1126/sciadv.ade5466.

Sharma, N., Spangenberg, J.E., Adatte, T., Vennemann, T., Kocsis, L., Vérité, J., Valero, L., and Castelltort, S., 2024, Middle Eocene Climatic Optimum (MECO) and its imprint in the continental Escanilla Formation, Spain: Climate of the Past, v. 20, p. 935–949, https://doi.org/10.5194/cp-20-935-2024.

Shen, J., Algeo, T.J., Planavsky, N.J., Yu, J., Feng, Q., Song, H., Song, H., Rowee, H., Zhou, L., and Chen, J., 2019, Mercury enrichments provide evidence of Early Triassic volcanism following the end-Permian mass extinction: Earth-Science Reviews, v. 195, p. 191–212, https://doi.org/10.1016/j.earscirev.2019.05.010.

Sluijs, A., Zeebe, R.E., Bijl, P.K., and Bohaty, S.M., 2013, A middle Eocene carbon cycle conundrum: Nature Geoscience, v. 6, p. 429–434, https://doi.org/10.1038/ngeo1807.

Them, T.R., II, Jagoe, C.H., Caruthers, A.H., Gill, B.C., Grasby, S.E., Gröcke, D.R., Yin, R.S., and Owens, J.D., 2019, Terrestrial sources as the primary delivery mechanism of mercury to the oceans across the Toarcian Oceanic Anoxic Event (Early Jurassic): Earth and Planetary Science Letters, v. 507, p. 62–72, https://doi.org/10.1016/j.epsl.2018.11.029.

Thibodeau, A.M., Ritterbush, K., Yager, J.A., West, A.J., Ibarra, Y., Bottjer, D.J., Berelson, D.J., Bergquist, B.A., and Corsetti, F.A., 2016, Mercury anomalies and the timing of biotic recovery following the end-Triassic mass extinction: Nature Communications, v. 7, 11147, https://doi.org/10.1038/ncomms11147.

van der Boon, A., Kuiper, K.F., van der Ploeg, R., Cramwinckel, M.J., Honarmand, M., Sluijs, A., and Krijgsman, W., 2021, Exploring a link between the Middle Eocene Climatic Optimum and Neotethys continental arc flare-up: Climate of the Past, v. 17, p. 229–239, https://doi.org/10.5194/cp-17-229-2021.

van der Ploeg, R., Selby, D., Cramwinckel, M.J., Li, Y., Bohaty, S.M., Middelburg, J.J., and Sluijs, A., 2018, Middle Eocene greenhouse warming facilitated by diminished weathering feedback: Nature Communications, v. 9, 2877, https://doi.org/10.1038/s41467-018-05104-9.

Westerhold, T., Röhl, U., Donner, B., and Zachos, J.C., 2018, Global extent of early Eocene hyperthermal events: A new Pacific benthic foraminiferal isotope record from Shatsky Rise (ODP Site 1209): Paleoceanography and Paleoclimatology, v. 33, p. 626–642, https://doi.org/10.1029/2017PA003306.

Westerhold, T., Marwan, N., Drury, A.J., Liebrand, D., Agnini, C., Anagnostou, E., Barnet, J.S.K., Bohaty, S.M., Vleeschouwer, D.D., Florindo, F., Frederichs, T., Hodell, D.A., Holbourn, A.E., Kroon, D., Lauretano, V., Littler, K., Lourens, L.J., Lyle, M., Pälike, H., Röhl, U., Tian, J., Wilkens, R.H., Wilson, P.A., and Zachos, J.C., 2020, An astronomically dated record of Earth's climate and its predictability over the last 66 million years: Science, v. 369, p. 1383–1387, https://doi.org/10.1126/science.aba6853.

Yang, M., Hou, G., and Shi, G., 2006, K-Ar geochronology of Cenozoic volcanic rocks of east Depression in Liaohe Basin and its geological significance: Beijing Da Xue Bao. Zi Ran Ke Xue Bao, v. 42, p. 184–191, https://doi.org/10.13209/j.0479-8023.2006.036.

Yao, Y., Liang, H., and Cai, Z., 1994, Tertiary in Petroliferous Regions of China IV, The Bohai Gulf Basin: Beijing, Petroleum Industry Press, 240 p.

Zhang, C., Liu, D., Liu, Q., Jiang, S., Wang, X., Wang, Y., Ma, C., Wu, A., Zhang, K., and Ma, Y., 2023, Magmatism and hydrocarbon accumulation in sedimentary basins: A review: Earth-Science Reviews, v. 244, 104531, https://doi.org/10.1016/j.earscirev.2023.104531.

Zhao, H., Shen, J., Algeo, T.J., Racki, G., Chen, J., Huang, C., Song, J., Qie, W., and Gong, Y., 2022, Mercury isotope evidence for regional volcanism during the Frasnian-Famennian transition: Earth and Planetary Science Letters, v. 581, 117412, https://doi.org/10.1016/j.epsl.2022.117412.

Printed in the USA